Nanotechnology

DOI: 10.1002/anie.200901723

Encapsulation of Sn@carbon Nanoparticles in Bamboo-like Hollow Carbon Nanofibers as an Anode Material in Lithium-Based Batteries**

Yan Yu, Lin Gu,* Chunlei Wang, Abirami Dhanabalan, Peter A. van Aken, and Joachim Maier*

In the past decades, considerable attention has been focused on electrochemical energy storage devices with both high energy and high power densities because of their potential applications in powering electric vehicles and portable electronic devices. Until now, rechargeable, so-called "Li-ion batteries" (LIBs) remain the most promising systems. It is still a major challenge to develop new materials and cells with high energy density, long cycle life, excellent rate capability performance, and environmental compatibility. To meet these requirements, substantial efforts have been made to develop new electrode materials and to design new structures of electrode materials.[1–10] As an anode material for LIBs, metallic tin (Sn) has attracted tremendous interest owing to its high theoretical capacity of about 990 mA h g^{-1} as $Li_{4.4}Sn$, which is significantly higher than that of graphitic carbon (372 mA h g^{-1} for LiC_6).[11–13] Nevertheless, practical implementation of metallic tin to LIBs is greatly hampered by the poor cyclability. One reason for the poor cycle life is the substantial volume changes that occur during charging and discharging, resulting in both mechanical failure and loss of electrical contact at the electrode. Another reason is the suspected tin nanoparticle aggregation during the discharging process.[14,15] The current strategies to overcome the so-called pulverization of Sn address three issues: reducing the alloy particle size, using composite materials, and selecting an optimized binder.[1,16,17] Various reports have demonstrated that the problems of volume change and metal particle aggregation can be significantly mitigated by using superfine intermetallic compounds and active/inactive composite alloy materials.[1,18–20] For example, nanostructured tin dispersed in a carbon matrix[21,22] has been shown to improve the cyclability of the tin anode considerably. Another approach to achieve improved electrochemical performance is to fabricate tin-based composites with hollow structures, which offers a "buffer zone" to compensate the volume fluctuation of the reactants, thus preserving the electrical pathways.[22–25] Recently, carbon-encapsulated hollow tin nanoparticles were reported as constituents of a superior anode material for LIB applications.[26,27] However, to the best of our knowledge, there have been only few reports on the one-step fabrication of Sn@carbon nanoparticles encapsulated in hollow carbon matrixes, especially in hollow carbon nanofibers.[23] Furthermore, it remains a great challenge to fabricate a metallic tin anode with excellent cyclability when the upper cutoff voltage is higher than 1.3 V.[1,28,29]

In this work, novel Sn@carbon nanoparticles encapsulated in bamboo-like hollow carbon nanofibers were prepared by pyrolysis of coaxially electrospun nanofibers.[30–32] Figure 1 a gives an overview of a typical coaxially electrospinning setup. In this work, two viscous liquids were simultaneously fed through the inner (core, containing tributyltin (TBT) and mineral oil solution) and outer (sheath, containing polyacrylonitrile (PAN) solution) capillaries, respectively. The flow rates of the two liquids were kept constant by two separate syringe pumps. When a high voltage is applied between the outer metallic capillary and the substrate, the jet formed by the outer solutions is stretched by electrostatic

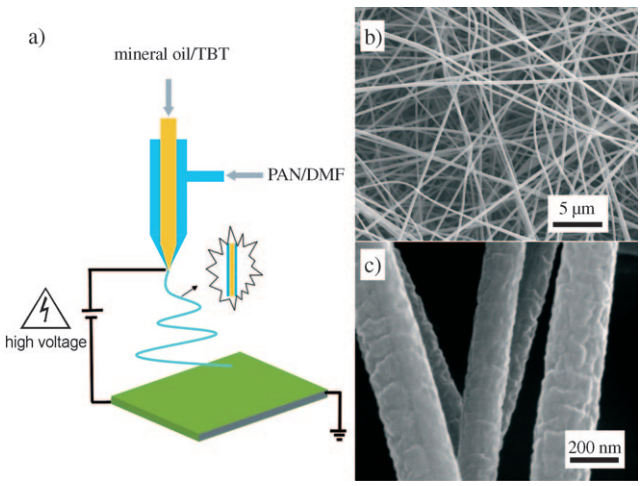

Figure 1. a) A homemade coaxial electrospinning spinneret used in preparing PAN/TBT core–sheath nanofibers. b) Overview and c) high-magnification SEM micrographs of porous as-collected PAN/TBT nanofibers obtained by coaxial electrospinning. The outer and inner fluids are 10 wt% PAN in DMF, and a mixture of mineral oil and TBT solution, respectively.

[*] Dr. Y. Yu, Prof. Dr. J. Maier
Max Planck Institute for Solid State Research
Heisenbergstrasse 1, 70569 Stuttgart (Germany)
E-mail: yan.yu@fkf.mpg.de
Dr. L. Gu, Priv.-Doz. P. A. van Aken
Stuttgart Center for Electron Microscopy,
Max-Planck Institute for Metals Research
Heisenbergstrasse 3, 70569 Stuttgart (Germany)
E-mail: gu@mf.mpg.de
Prof. C. Wang, A. Dhanabalan
Department of Mechanical and Materials Engineering
Florida International University
Miami, FL 33174 (USA)

[**] We acknowledge financial support from the US Air Force (FA9550-07-1-0344 and FA9550-08-1-0287) and the European Union under the Framework 6 program under a contract for an Integrated Infrastructure Initiative ESTEEM Reference 026019. Y.Y. is grateful for a scholarship from the Alexander von Humboldt foundation.
Supporting information for this article is available on the WWW under http://dx.doi.org/10.1002/anie.200901723.

forces to generate coaxial nanofibers. Subsequently, as described in Scheme 1, the as-collected nanofibers were immersed in *n*-octane for more than 12 h to extract the mineral oil for the hollow nanostructure. Finally, after soaking, the nanofibers were pyrolyzed at 1000 °C for 5 h

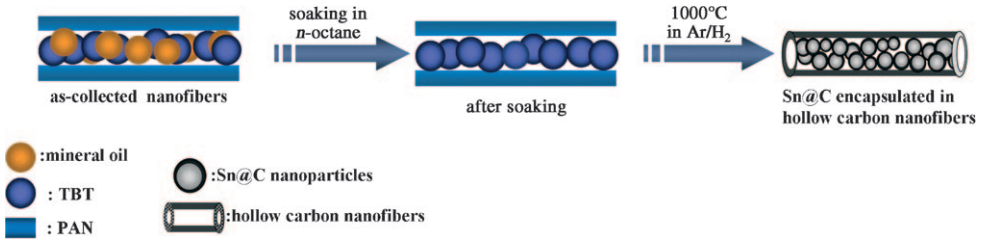

Scheme 1. Preparation of Sn@carbon nanoparticles encapsulated in hollow carbon nanofibers.

under Ar (95 vol %)/H_2 (5 vol %) atmosphere to carbonize the outer PAN (sheath); meanwhile the inner TBT solution was decomposed to form the Sn@carbon nanoparticles (core) encapsulated in hollow carbon nanofibers.

The first novel feature of our study is the in situ formation of Sn@carbon nanoparticles encapsulated in bamboo-like hollow carbon nanofibers by pyrolysis of electrospun TBT (core)/PAN (sheath) nanofibers. This novel Sn/C composite shows a reversible capacity as high as 737 mA h g^{-1}, while maintaining outstanding cyclability, for Li storage in the voltage window of 0.01–3.0 V at 0.5 C. The charge retention was measured to be 90 % of the original value after 200 cycles. The specific structure of this Sn/C composite plays an important role in optimizing and even enhancing the electrochemical performance of the Sn component. First, the thin carbon layer coated on the surface of tin nanoparticles increases the conductivity and additionally buffers the large volume change during cycling. The cyclability of the Sn/C composite is thus enhanced too. Second, the Sn@carbon structure is further encapsulated in hollow carbon nanofibers, which offers adequate void space to digest the large volume change, preventing the electrical isolation after prolonged cycle time. Furthermore, the dual carbon protection prevents the encapsulated metallic tin from oxidation to form tin oxide, and also improves the electronic conductivity.

The as-collected nanofibers display fibrous morphology, as shown in a secondary electron image (Figure 1 b) obtained by field-emission scanning electron microscopy (FE-SEM). Continuous nanofibers of uniform diameter were revealed. Figure 1 c shows a magnified view of these fibers, and the average diameter was measured to be (200 ± 50) nm. The surfaces of these fibers are rough, which is attributed to solvent evaporation during the long electrospinning process. X-ray diffraction (XRD) analysis of the pyrolyzed Sn/C nanofibers clearly reveals the diffraction patterns of β-Sn (JCPDS; No. 86-2265), (see the Supporting Information, Figure S1). No tin oxide was detected.

Transmission electron microscopy (TEM) analyses of the pyrolyzed Sn@carbon nanoparticles encapsulated in hollow carbon nanofibers provide worthwhile structural and chemical information. Figure 2 a shows a bright-field (BF) zero-loss energy-filtered image of the pyrolyzed nanofibers. The encapsulation of tin nanoparticles in bamboo-like hollow carbon nanofibers is clearly revealed. It is believed that the formation of a bamboo-like structure results from the incorporation of nitrogen from PAN into the carbon nanotubes.[33] The diameters of the hollow carbon nanofibers were measured to be about 150 nm, which is less than that of the as-collected nanofibers. The main reason for this contraction is the decomposition of organic components of PAN. To distinguish metallic tin from hollow carbon nanofibers, energy-filtered imaging was performed. Figure 2 b shows the elemental mapping of carbon (blue) and tin (yellow) using the characteristic energy-losses of the tin N edges at 32 eV and the carbon σ + π plasmons at 24 eV. Both energy-filtered images were divided by the zero-loss image to remove possible elastic contrast. The embedded tin nanoparticle size was measured to be about 100 nm. A BF electron micrograph obtained from an isolated Sn@carbon nanoparticle encapsulated in a hollow carbon nanofiber is shown in Figure 2 c. A thin layer of graphitic carbon with a thickness of about 10 nm was observed surrounding the surface of a metallic tin particle. The

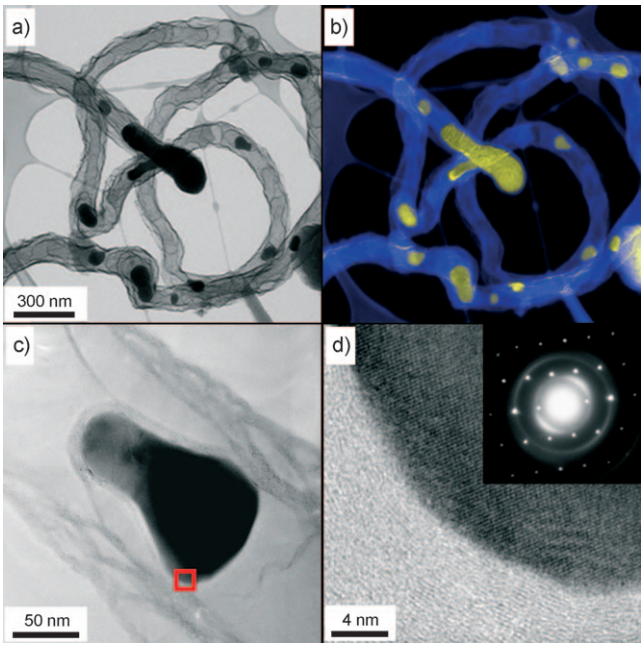

Figure 2. a) BF zero-loss filtered elastic TEM micrograph of the pyrolyzed nanofibers obtained by calcining the composite in Ar/H_2 at 1000 °C for 5 h; b) elemental mapping of the nanofibers showing the chemical distribution of carbon (blue) and tin (yellow); c) BF electron micrograph of an isolated Sn@carbon nanoparticle encapsulated in a hollow carbon nanofiber; d) HRTEM and SAED (inset) images of the region marked in (c) indicate the presence of single-crystalline metallic tin and graphitic carbon.

thickness of the outer-wall, hollow graphitic carbon fiber was measured to be about 30 nm. High-resolution transmission electron microscopy (HRTEM) and selected area electron diffraction (SAED), shown in Figure 2d and the inset of Figure 2d, respectively, were performed at the region marked in Figure 2c. Both HRTEM and SAED investigations confirm the presence of single-crystalline metallic tin and graphitic carbon. The formation of this specific structure can be understood as follows. The graphitic carbon layer (ca. 10 nm) surrounding Sn nanoparticles originates from the decomposition of inner TBT solutions. A similar result has been reported previously.[21] Subsequently, the Sn@carbon nanoparticles were encapsulated in the hollow carbon nanofibers resulting from the pyrolysis of PAN at 1000 °C for 5 h under Ar/H_2 atmosphere. EDX analysis (see the Supporting Information, Figure S2 and Table S1) reveals that the Sn/C composite contains approximately 32 wt % carbon, 66 wt % tin, and trace amounts of oxygen.

Figure 3a shows cyclic voltammograms of Sn@carbon nanoparticles encapsulated in hollow carbon nanofibers. Two waves at 0.44 and 0.21 V were observed during the first discharge, attributed to lithium alloying with tin forming Li_xSn alloys.[34] Furthermore, the absence of peaks at 1.05 or 1.55 V implies that Sn was encapsulated in a carbon shell.[34] The difference between the first and later cycles is partly ascribed to formation of a solid-electrolyte-interphase (SEI) layer. Figure 3b displays the voltage profiles of electrochemical cells made of these Sn/C composites at a rate of 0.1 C (50 mA g^{-1}), (that is, discharging the theoretical capacity in 10 h) in the voltage range of 0.01–3.0 V (vs. Li). This voltage profile indicates that the composite electrode exhibits the typical characteristics of an Sn electrode. The first discharge and charge steps deliver a specific capacity of 1156 and 824 mA h g^{-1}, respectively. The large initial capacity loss of the Sn/C composite electrode can be partly attributed to the formation of a thick SEI layer on the electrode surface during the first discharge step,[1,24,28] and the storage of Li^+ in hollow carbon nanofibers, which are difficult to be extracted.[27] Theoretically, a complete discharge process completes the reactions (1) and (2), corresponding to a theoretical discharge capacity of 806 mA h g^{-1}.

$$Sn + 4.4\,Li \rightarrow Li_{4.4}Sn \quad (1)$$

$$6\,C + Li \rightarrow LiC_6 \quad (2)$$

To obtain further evidence of the improved performance of our Sn/C composite electrode, we tested the cycling performance of a commercial Sn nanopowder electrode with a composite of similar particle size (100 nm) under the

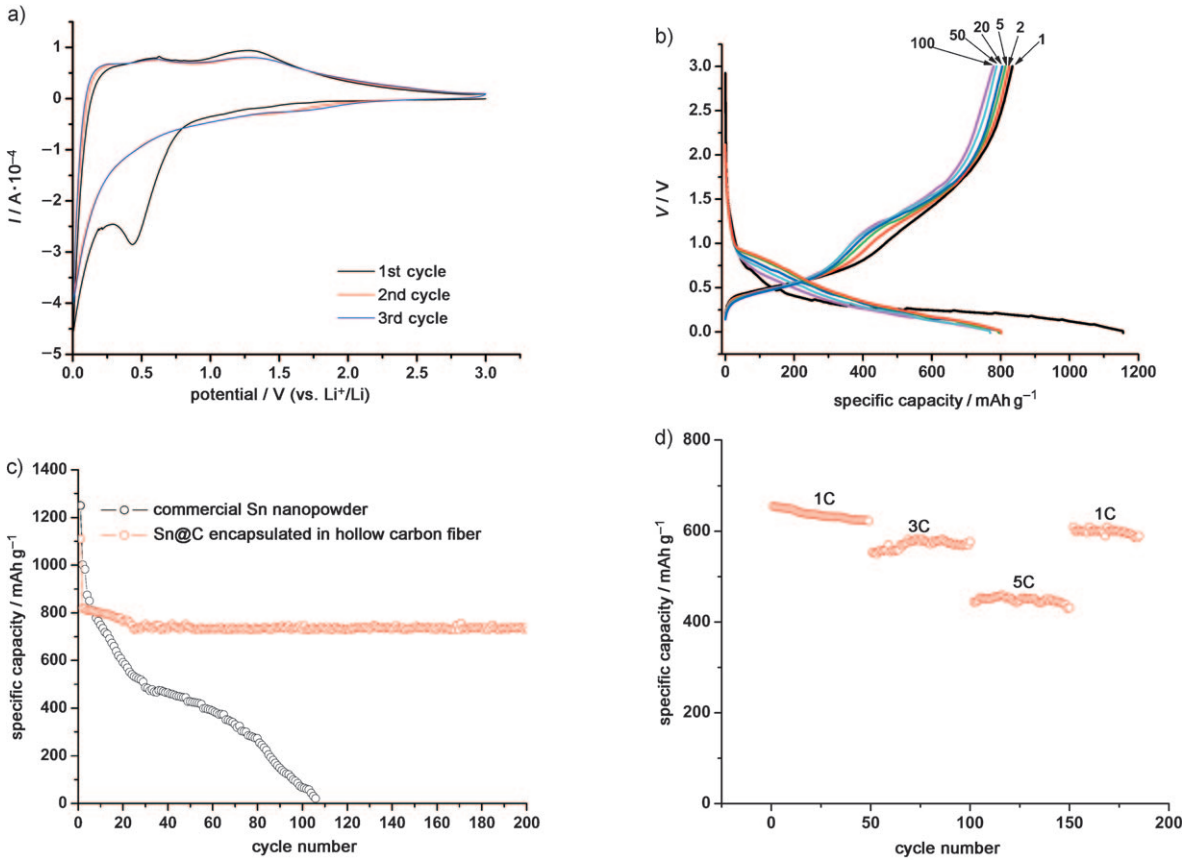

Figure 3. a) Cyclic voltammograms of Sn@carbon nanoparticles encapsulated in bamboo-like hollow carbon nanofibers electrode; scan speed 0.2 mV s^{-1}. b–d) Electrochemical performance of Sn/C composite electrode cycled between 0.01 and 3 V vs. Li^+/Li. b) Voltage profiles of a Sn/C composite electrode at a cycling rate of 0.1 C; the cycle numbers are shown. c) Capacity–cycle number curves of a Sn/C composite electrode and a commercial Sn nanopowder (diameter: 100 nm) electrode at a cycling rate of 0.5 C; d) Discharge capacity of a Sn/C composite electrode as a function of discharge rate (1–5 C).

same conditions. Figure 3c shows the curves of discharge capacity versus cycle number for the Sn/C composite electrode and the commercial Sn nanopowder electrode at a rate of 0.5 C. The Sn/C composite electrode exhibits improved cyclic performance and a higher reversible specific capacity of over 800 $mA\,h\,g^{-1}$ in the first 10 cycles and maintains a reversible capacity after 200 cycles of approximately 737 $mA\,h\,g^{-1}$, which corresponds to 91% of the theoretical capacity. Although an electrode made of commercial Sn nanopowder electrode delivered a high discharge capacity for the initial 40 cycles, subsequently it drops rapidly probably because of disconnection of the material. The improved cyclability of the Sn/C composite electrode is based on its specific structure that provides the following benefits: 1) The first shell of carbon hollow fibers offers adequate void space, which acts as a "buffer zone" to accommodate the large volume change in the lithiation and delithiation processes. 2) The second shell coated on the surface of Sn nanoparticles prevents the Sn particles from aggregation, leading to alleviation of the pulverization after long time cycling. 3) All Sn@carbon nanoparticles encapsulated in carbon hollow fibers provide higher specific surface area, which improves the electrical contact as well as lithium ion conduction.

Figure 3d shows the rate capability of the Sn/C composite electrode: it delivers a rate capacity of about 650 $mA\,h\,g^{-1}$, when first cycled at 1 C, 550 $mA\,h\,g^{-1}$ at 3 C, 480 $mA\,h\,g^{-1}$ at 5 C, and finally back to 610 $mA\,h\,g^{-1}$ at 1 C again. The improved electrochemical performance of the Sn/C composite electrode is probably rooted in its special morphology. Moreover, the nanostructured tin particles shorten the transport lengths for both electrons and lithium ions; the unique hollow structure ensures a high electrode–electrolyte contact area and enables to digest the volume change during charge/discharge processes. In addition, the entire fabrication procedure is straightforward and high-yielding. The diameter and thickness of hollow carbon fibers can be readily tuned by adjusting the co-electrospinning parameters (e.g. concentration of PAN solution, flow rate of the PAN solution, and the electrical field).

In summary, a Sn/C composite structure, namely Sn@carbon encapsulated in bamboo-like hollow carbon nanofibers, was fabricated by pyrolysis of TBT (core)/PAN (sheath) nanofibers through a coaxial electrospinning method. As a potential anode material for LIBs, this composite displays a high reversible capacity of 737 $mA\,h\,g^{-1}$ after 200 cycles at 0.5 C. It also exhibits a reversible discharge capacity as high as 480 $mA\,h\,g^{-1}$ when cycled at 5 C . The particular Sn@carbon encapsulated in hollow carbon nanofibers structure has high Sn content (close to 70 wt% Sn and 30 wt% carbon) and provides appropriate void volume to respond to the large volumes change and to prevent pulverization of the Sn nanoparticles. This composite is very promising as a potential anode material for LIBs even though the kinetics of the charge process requires further improvement. Moreover, coaxial electrospinning has proved itself to be a powerful routine for the preparation of nanomaterials with hollow core/shell architectures.

Experimental Section

Materials: A polyacrylonitrile (PAN, MW = 150000, Aldrich) solution with a concentration of 10 wt% was used as the outer fluid during the coaxial electrospinning process. The solution was prepared by dissolving PAN powder (1 g) in *N*,*N*-dimethylformamide (DMF, 10 g) (99.8%, Aldrich) at 80°C with vigorous stirring. The inner fluid was a mixture of mineral oil (98%, Aldrich), and tributyltin (TBT) (96%, Aldrich). The weight ratio of TBT and mineral oil was 1:1.

Electrospinning: The setup for coaxial electrospinning is depicted in Figure 1a. In brief, the spinneret consists of two stainless-steel tubes with the diameters of 1.2 mm (outer) and 0.5 mm (inner). Both tubes are 0.1 mm thick and are placed coaxially. A piece of grounded thin copper plate was placed 15 cm below the spinneret to collect the nanofibers. A high voltage of 20 kV was supplied at the spinneret by a direct-current power supply (Gamma High Voltage, ES30P). The two liquids obtained above were fed using two syringe pumps (KDS-200, Stoelting, Wood Dale, 1 L). The typical feeding rates for the outer (PAN) and inner solution (mineral oil and TBT) were set at 15 and 5 $\mu L\,min^{-1}$, respectively. All experiments were conducted at room temperature in air.

Synthesis of Sn@carbon nanoparticles encapsulated in hollow carbon fibers: The collected electrospun nanofibers were soaked in *n*-octane for more than 12 h to extract the mineral oil and obtain the hollow carbon nanofiber structures. The electrospun nanofibers were then put in a tube furnace and calcined at 1000°C in Ar (95 vol%)/H_2 (5 vol%) for 5 h to obtain Sn/C composite nanofibers. The heating rate was 2°C min^{-1}.

Characterization: The composition and crystal structures of the annealed Sn/C nanofibers were obtained by X-ray diffraction (XRD) analysis. The surface morphology was investigated using a JEOL 6300F field-emission scanning electron microscope (JEOL, Tokyo, Japan) operating at 15 keV. High-resolution transmission electron microscopy was performed using a JEOL 4000EX transmission electron microscope (JEOL, Tokyo, Japan) operating at 400 keV. The interpretable resolution defined by the contrast transfer function of the objective lens was 0.16 nm. Energy-dispersive X-ray spectroscopy (EDX) analysis was carried out using an EDAX system (EDAX, Mahwah, NJ, USA) attached to a Zeiss SESAM (Carl Zeiss, Oberkochen, Germany) microscope operating at 200 keV. Chemical mapping was also performed using the SESAM microscope equipped with an electrostatic Ω-type monochromator and a MANDOLINE filter, which provides a routinely achievable energy resolution of better than 100 meV.

Electrochemical characterization: The electrospun Sn/C composite, carbon black, and poly(vinyl difluoride) (PVDF) were mixed in a weight ratio of 70:15:15. The obtained slurry was pasted on copper foil using the doctor blade technique to prepare the electrode film (the thickness of slurry was controlled as 100 μm by adjusting the gap of doctor blade), followed by dehydration in a vacuum oven for 12 h. The thickness of dried electrode film was approximately 92 μm. A typical electrode disk ($\Phi = 10$ mm) weighed 5.2 mg, which corresponds to an active material mass loading of 6.6 $mg\,cm^{-2}$. The obtained films were used as the electrodes of electrochemical cells Sn/C/Li with 1M $LiPF_6$ in ethylene carbonate and diethyl carbonate (EC-DEC, v/v = 1:1) as the electrolyte. Celgard 2400 was used as a separator film. Pure lithium foil (99.9%, Aldrich) was used as the counter electrode and reference electrode. The cells were assembled in an argon-filled glove box (MBRAUN LABMASTER 130), where moisture and oxygen levels were kept below 1 ppm. Electrochemical experiments were performed using Swagelok-type cells, which were cycled in the voltage range between 3.0 V and 0.01 V with a battery test system (Arbin MSTAT system).

Received: March 30, 2009
Revised: May 20, 2009
Published online: July 23, 2009

Keywords: electrochemistry · electrospinning · lithium · tin

[1] Y. Idota, T. Kubota, A. Matsufuji, Y. Maekawa, T. Miyasaka, *Science* **1997**, *276*, 1395.
[2] J. M. Tarascon, P. Poizot, S. Laruelle, S. Grugeon, L. Dupont, *Nature* **2000**, *407*, 496.
[3] A. S. Arico, P. Bruce, B. Scrosati, J. M. Tarascon, W. van Schalkwijk, *Nat. Mater.* **2005**, *4*, 366.
[4] J. Maier, *Nat. Mater.* **2005**, *4*, 805.
[5] A. M. Cao, J. S. Hu, H. P. Liang, L. J. Wan, *Angew. Chem.* **2005**, *117*, 4465; *Angew. Chem. Int. Ed.* **2005**, *44*, 4391.
[6] Y. Wang, J. Y. Lee, H. C. Zeng, *Chem. Mater.* **2005**, *17*, 3899.
[7] J. Chen, L. Xu, W. Li, X. Gou, *Adv. Mater.* **2005**, *17*, 582.
[8] Y. S. Hu, L. Kienle, Y. G. Guo, J. Maier, *Adv. Mater.* **2006**, *18*, 1421.
[9] Y. G. Guo, Y. S. Hu, J. Maier, *Chem. Commun.* **2006**, 2783.
[10] X. W. Lou, Y. Wang, C. Yuan, J. Y. Lee, L. A. Archer, *Adv. Mater.* **2006**, *18*, 2325.
[11] M. Winter, G. H. Wrodnigg, J. O. Besenhard, W. Biberacher, P. Novak, *J. Electrochem. Soc.* **2000**, *147*, 2427.
[12] I. A. Courtney, J. R. Dahn, *J. Electrochem. Soc.* **1997**, *144*, 2045.
[13] M. Winter, J. O. Besenhard, *Electrochim. Acta* **1999**, *45*, 31.
[14] S. Grugeon, S. Laruelle, R. Herrera-Urbina, L. Dupont, P. Poizot, J. M. Tarascon, *J. Electrochem. Soc.* **2001**, *148*, A285.
[15] E. Shembel, R. Apostolova, V. Nagirny, I. Kirsanova, Ph. Grebenkin, P. Lytvyn, *J. Solid State Electrochem.* **2005**, *9*, 96.
[16] N. Li, C. R. Martin, *J. Electrochem. Soc.* **2001**, *148*, A164.
[17] M. Wachtler, M. R. Wagner, M. Schmied, M. Winter, J. O. Besenhard, *J. Electroanal. Chem.* **2001**, *510*, 12.
[18] J. O. Besenhard, J. Yang, M. Winter, *J. Power Sources* **1997**, *68*, 87.
[19] J. Y. Lee, R. Zhang, Z. Liu, *Electrochem. Solid-State Lett.* **2000**, *3*, 167.
[20] J. Yang, M. Wachtler, M. Winter, J. O. Besenhard, *Electrochem. Solid-State Lett.* **1999**, *2*, 161.
[21] G. L. Cui, Y. S. Hu, L. J. Zhi, D. Q. Wu, I. Frieberwirth, J. Maier, K. Müllen, *Small* **2007**, *3*, 2066.
[22] Z. W. Zhao, Z. P. Guo, P. Yao, H. K. Liu, *J. Mater. Sci. Technol.* **2008**, *24*, 657.
[23] K. T. Lee, Y. S. Jung, S. M. Oh, *J. Am. Chem. Soc.* **2003**, *125*, 5652.
[24] Y. Wang, H. C. Zeng, J. Y. Lee, *Adv. Mater.* **2006**, *18*, 645.
[25] H. Qiao, Z. Zheng, L. Zhang, L. Xiao, *J. Mater. Sci.* **2008**, *43*, 2778.
[26] W. M. Zhang, J. S. Hu, Y. G. Guo, S. F. Zheng, L. S. Zhong, W. G. Song, L. J. Wan, *Adv. Mater.* **2008**, *20*, 1160.
[27] D. Deng, J. Y. Lee, *Angew. Chem.* **2009**, *121*, 1688; *Angew. Chem. Int. Ed.* **2009**, *48*, 1660.
[28] Y. W. Xiao, J. Y. Lee, A. S. Yu, Z. L. Liu, *J. Electrochem. Soc.* **1999**, *146*, 3623.
[29] Y. Yan, C. H. Chen, Y. Shi, *Adv. Mater.* **2007**, *19*, 993.
[30] X. X. Wang, J. N. Wang, H. Chang, Y. F. Zhang, *Adv. Funct. Mater.* **2007**, *17*, 3613.
[31] Z. Sun, E. Zussman, A. L. Yarin, J. H. Wendorff, A. Greiner, *Adv. Mater.* **2003**, *15*, 1929.
[32] E. Zussman, A. L. Yarin, A. V. Bazilevsky, R. Avrahami, M. Feldman, *Adv. Mater.* **2006**, *18*, 348.
[33] B. G. Sumpter, V. Meunier, J. M. Romo-Herrera, E. Cruz-Silva, D. A. Cullen, H. Terrones, D. J. Smith, M. Terrones, *ACS Nano* **2007**, *1*, 369.
[34] Y. S. Jung, K. T. Lee, J. H. Ryu, D. Im, S. M. Oh, *J. Electrochem. Soc.* **2005**, *152*, A1452.

